

Virology

Congenital Zika syndrome is associated with maternal protein malnutrition

J. Barbeito-Andrés^{1,2}, P. Pezzuto³, L. M. Higa³, A. A. Dias⁴, J. M. Vasconcelos⁵, T. M. P. Santos⁶, J. C. C. G. Ferreira¹, R. O. Ferreira¹, F. F. Dutra⁴, A. D. Rossi³, R. V. Barbosa⁷, C. K. N. Amorim⁸, M. P. C. De Souza⁸, L. Chimelli⁹, R. S. Aguiar³, P. N. Gonzalez², F. A. Lara¹⁰, M. C. Castro¹¹, Z. Molnár¹², R. T. Lopes⁶, M. T. Bozza⁴, J. L. S. G. Vianez⁸, C. G. Barbeito¹³, P. Cuervo¹⁰, M. Bellio⁴, A. Tanuri³, P. P. Garcez^{1*}

Copyright © 2020
The Authors, some
rights reserved;
exclusive licensee
American Association
for the Advancement
of Science. No claim to
original U.S. Government
Works. Distributed
under a Creative
Commons Attribution
NonCommercial
License 4.0 (CC BY-NC).

Zika virus (ZIKV) infection during pregnancy is associated with a spectrum of developmental impairments known as congenital Zika syndrome (CZS). The prevalence of this syndrome varies across ZIKV endemic regions, suggesting that its occurrence could depend on cofactors. Here, we evaluate the relevance of protein malnutrition for the emergence of CZS. Epidemiological data from the ZIKV outbreak in the Americas suggest a relationship between undernutrition and cases of microcephaly. To experimentally examine this relationship, we use immunocompetent pregnant mice, which were subjected to protein malnutrition and infected with a Brazilian ZIKV strain. We found that the combination of protein restriction and ZIKV infection leads to severe alterations of placental structure and embryonic body growth, with offspring displaying a reduction in neurogenesis and postnatal brain size. RNA-seq analysis reveals gene expression deregulation required for brain development in infected low-protein progeny. These results suggest that maternal protein malnutrition increases susceptibility to CZS.

INTRODUCTION

By the end of 2015, a severe Zika virus (ZIKV) outbreak in the Americas was followed by a steep increase in primary microcephaly (1). The causal relationship between ZIKV and brain malformations was confirmed by in vitro studies showing that ZIKV exposure directly infects human neural progenitors (2, 3) and impairs the growth of three-dimensional differentiating cultures (3) while altering genes (2) and proteins related to cell cycle arrest (4). In vivo, vertical ZIKV transmission was modeled mainly by using immunocompromised mice, which are susceptible to this viral infection (5, 6). Severe reduction of brain size is considered the hallmark of what is now called the congenital Zika syndrome (CZS), a collection of developmental malformations associated with ZIKV's congenital infection such as ventriculomegaly, calcifications, corpus callosum agenesis, lissencephaly, and retinal abnormalities (7).

As with other STORCH (syphilis, toxoplasmosis, others, rubella, cytomegalovirus, and herpes virus) pathogens, ZIKV infection during pregnancy leads to birth defects in some but not all affected mothers. Approximately 6 to 12% of infected pregnancies will result in CZS (8). The distribution of CZS in human populations, however, is

asymmetrical (9). In Brazil, which has reported ~95% of all CZS cases (1) and where ZIKV has severely affected multiple states, most occurrences of CZS (~75%) were found in the disadvantaged socioeconomic region of the Northeast (1, 10). Epidemiological surveys showed that, even within Northeastern communities, ZIKV-related microcephaly was most prevalent in those areas with the lowest socioeconomic status (11). Hence, cofactors are likely to play a key role in modulating ZIKV infection's severity and the level of developmental impairment.

Malnutrition is considered one of the most critical causes of immunodeficiency worldwide (12), as it can substantially increase a host's susceptibility to an infection and amplify pathogenesis severity (13). An insufficient intake of protein can be a form of undernutrition and is a widespread problem in low-income populations, which have limited access to more expensive food components (14).

Here, by analyzing epidemiological data collected in Brazil from the ZIKV outbreak period, we found a significant prevalence of microcephaly in states where undernutrition is more frequent. To experimentally assess this correlation, we developed a mouse model using immunocompetent pregnant females, which were infected with ZIKV at the peak of embryonic neurogenesis and were exposed to protein restriction before and during gestation. Using this undernourished mouse model, we identified that there is robust and persistent ZIKV infection in the spleens of undernourished mothers, in contrast to controls. We also found severe alterations of placental structure and embryonic body growth compromise in addition to the decline of embryonic neurogenesis and reduction in brain size of newborns. From RNA sequencing (RNA-seq) analysis, we conclude that the significant differences in the regulation patterns of key pathways and particular genes identified within developing brains reflect how a poor nutritional status increases the adverse effects of ZIKV infection. Together, these data provide important new clues to understand the impact of environmental cofactors and, particularly, nutrition in the emergence of CZS.

¹Institute of Biomedical Sciences, Federal University of Rio de Janeiro, Rio de Janeiro, Brazil. ²Institute for Studies in Neuroscience and Complex Systems (ENyS) CONICET, Buenos Aires, Argentina. ³Department of Genetics, Institute of Biology, Federal University of Rio de Janeiro, Rio de Janeiro, Brazil. ⁴Microbiology Institute Paulo de Góes, Federal University of Rio de Janeiro, Rio de Janeiro, Brazil. ⁵Biological Science Institute, Federal University of Pará, Belém, Brazil. ⁶Nuclear Instrumentation Laboratory, Federal University of Rio de Janeiro, Rio de Janeiro, Brazil. ⁷CENABIO (National Center of Structural Biology and Bioimaging), Rio de Janeiro, Brazil. ⁸Technological Innovations Centre, Evandro Chagas Institute, Ananindeua, Brazil. ⁹State Institute of Brain Paulo Niemeyer, Rio de Janeiro, Brazil. ¹⁰Oswaldo Cruz Institute, Fiocruz, Rio de Janeiro, Brazil. ¹¹Department of Global Health and Population, Harvard T. H. Chan School of Public Health, Boston, MA, USA. ¹²Department of Physiology, Anatomy and Genetics, University of Oxford, Oxford, UK. ¹³Faculty of Veterinary Sciences, National University of La Plata, Buenos Aires, Argentina.

*Corresponding author. Email: ppgarcez@icb.ufrj.br

RESULTS

Microcephaly during ZIKV Brazilian outbreak is more prevalent in regions where undernutrition is endemic

First, we explored the potential relationship between undernutrition and microcephaly associated with ZIKV through correlation analysis using the Brazilian Ministry of Health's integrated data bank. We focused on those states that occupied the tropical part of the country (24 of the 27 Brazilian states) since ZIKV has been more frequent there because of the abundance of its main vector, the *Aedes* mosquitoes. To study the hypothesized relationship, we then considered the number of cases of microcephaly that were confirmed and those still under investigation in the relevant states between 2015 and 2018 and quantified the number of undernourished patients admitted to hospitals for the same states between 2009 and 2018. Considering this catchment area, a significant positive correlation was found to exist between cases of microcephaly and occurrences of under-

nourishment ($r = 0.4$, $P = 0.05$) (Fig. 1A). Since this correlation, although significant, is subtle, we used a probabilistic simulation approach to test whether the observed pattern is significant. The observed correlation coefficient resulted in $r = 0.4$, and the P -adjusted value derived from the Monte Carlo simulation was 0.028 (fig. S1). In other words, this result supports the positive correlation identified between cases of microcephaly and undernutrition within the dataset, suggesting that states characterized by a higher number of cases with undernutrition over the past decade also exhibit more patients with microcephaly since the emergence of CZS in Brazil (Fig. 1A and table S1). Note that CZS cases are concentrated in some regions, although ZIKV infections were spread broader (fig. S2), confirming the asymmetrical geographical distribution previously reported (9).

To examine this association in more detail, we interviewed 83 mothers of children with CZS from Ceará state (northeast of Brazil) about their dietary consumption during pregnancy. They were asked

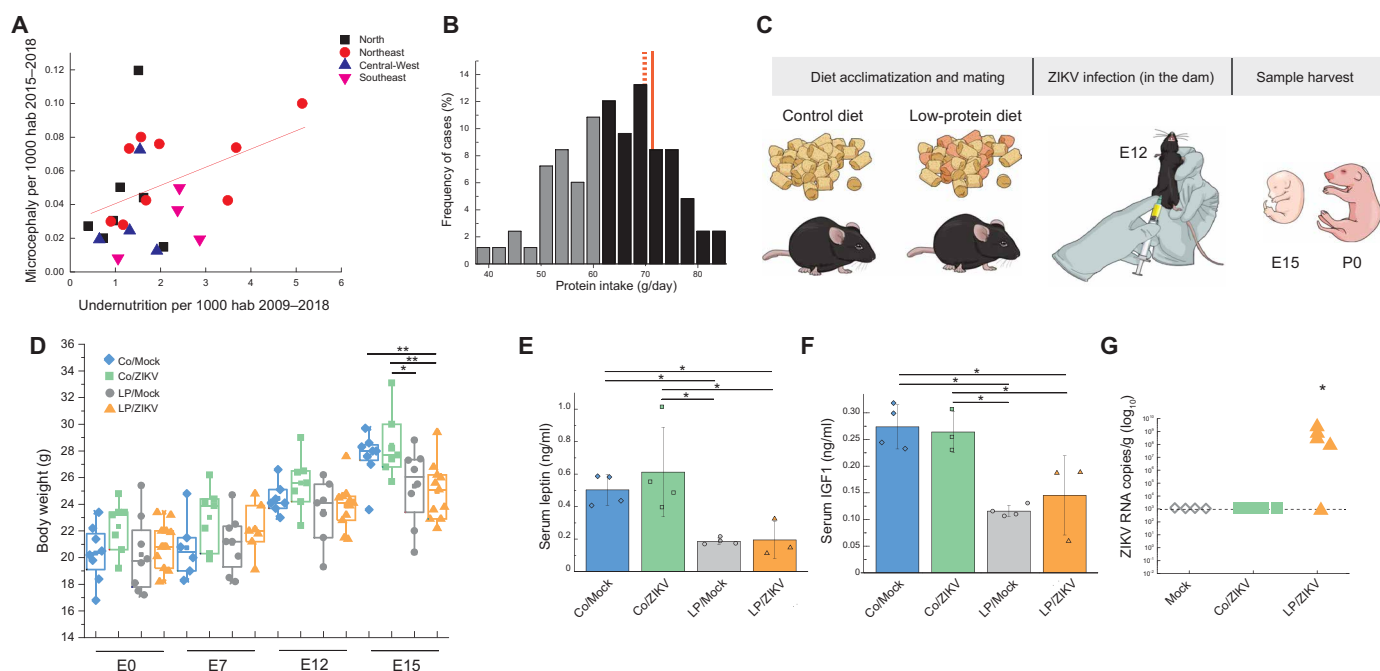


Fig. 1. Protein malnutrition reduces maternal body weight and enhances ZIKV load. (A) Relationship between undernutrition, measured as the number of hospitalized cases due to any undernutrition, and microcephaly cases that were confirmed or under investigation in Brazil since the first American ZIKV outbreak. Taking into consideration the data of 24 tropical states, a significant positive correlation was found between these variables (Pearson correlation: $r = 0.4$, P -adj = 0.028). Each symbol represents a Brazilian tropical state. Geographical regions to which these states belong are indicated. hab, inhabitants. (B) Distribution of daily protein consumption of interviewed mothers with CZS children. Those that were under the recommended amount of protein intake are in gray, and those who achieved values above recommendations are in black. Those mothers considered under protein restriction consumed 53.86 ± 5.49 g/day on average. Red lines indicate the daily average protein intake for the Northeast region (solid line) and particularly for the state of Ceará (dashed line). Mothers from Ceará have a mean protein intake significantly larger than CZS interviewed mothers ($t = -7.5$, $P < 0.001$). (C) Schematic description of experimental groups and infection protocol. Wild-type dams were divided into control (Co) diet and low-protein diet (LP), and at E12, they were intraperitoneally injected either with 10^6 PFU of a Brazilian ZIKV strain from a stock with 3.4×10^6 PFU/ml (injected volume, 295 μ l) or with the supernatant of *Aedes albopictus* C6/36 cells (Mock). P0, postnatal day 0. (D) Quantification of maternal body weight during pregnancy (n of dams per group: Co/Mock, 8; Co/ZIKV, 6; LP/Mock, 8; and LP/ZIKV, 11). Differences in maternal weight were only registered at E15 [Kruskal-Wallis, 11.375 (**)] [multiple comparisons with Mann-Whitney U : Co/Mock versus Co/ZIKV, $Z = 0.000$; Co/Mock versus LP/Mock, $Z = -1.892$; Co/Mock versus LP/ZIKV, $Z = -2.522$ (**); Co/ZIKV versus LP/Mock, $Z = -2.027$ (*); Co/ZIKV versus LP/ZIKV, $Z = -2.720$ (**); and LP/Mock versus LP/ZIKV, $Z = -0.496$]. Total leptin (E) and insulin-like growth factor 1 (IGF1) (F) maternal serum levels were measured by specific murine enzyme-linked immunosorbent assay (ELISA) at E15. The levels of both hormones were significantly lower only in LP groups than in Co diet groups [n per group: Co/Mock = 4; Co/ZIKV = 4 (leptin)/3 (IGF1); LP/Mock = 4; and LP/ZIKV = 3] [Kruskal-Wallis (leptin), 10.617 (*); multiple comparisons with Mann-Whitney U : Co/Mock versus LP/Mock, $Z = -2.309$ (*); Co/Mock versus LP/ZIKV, $Z = -2.121$ (*); Co/ZIKV versus LP/Mock, $Z = -2.309$ (*); and Co/ZIKV versus LP/ZIKV, $Z = -2.121$ (*)] [Kruskal-Wallis (IGF1), 9.967 (*); multiple comparisons with Mann-Whitney U : Co/Mock versus LP/Mock, $Z = -2.309$ (*); Co/Mock versus LP/ZIKV, $Z = -2.121$ (*); Co/ZIKV versus LP/Mock, $Z = -2.121$ (*); and Co/ZIKV versus LP/ZIKV, $Z = -1.964$ (*)]. The error bar represents mean \pm SD. (G) Viral load was quantified by RT-qPCR on E15 maternal spleen and expressed as ZIKV RNA copies per gram (n of dams per group: Mock = 4; Co/ZIKV = 4; and LP/ZIKV = 5). High levels of ZIKV RNA were found in most of LP/ZIKV spleen tissues [Mann-Whitney U : Co/ZIKV versus LP/ZIKV, $Z = -2.147$ (*)]. * $P < 0.05$, ** $P < 0.01$, and $P > 0.05$.

to indicate how many times a week they ate different types of foods. From these reports, the daily consumption of each macronutrient was estimated. We found that 37.35% of participants had a protein intake below 61 g/day (Fig. 1B and table S2), which is considered a protein-deficient diet for pregnant women (15). This is in agreement with previous studies that have identified the differential prevalence of maternal protein malnutrition in Brazilian regions such as the Northeast (27.3%) (16), the Southeast (12%) (17), and the South (2.85%) (18). Compared to data from the Brazilian Institute of Geography and Statistics [Instituto Brasileiro de Geografia e Estatística (IBGE)], on average, the protein intake in our sample is 64.14 g/day, lower than the reported state and regional values, 69.54 and ~71.00 g/day, respectively (Fig. 1B). The difference between the mean protein intake from the surveyed mothers of CZS babies and the reference for Ceará state is statistically significant (Fig. 1B). Furthermore, the overall distribution of protein intake levels in the survey is skewed toward lower levels. On the basis of these results, the relative risk was estimated by using the odd ratio formula, which compares the proportion of cases under or above the suggested protein intake of the interviewed mothers against that referenced by Ceará state. The resulting odd ratio of 1.5 indicates that there is a trend for CZS to be more probable in the protein-restricted group than in the well-nourished group of mothers (table S3). However, confidence intervals for the 95% of the distribution are 0.96 to 2.34, and the odd ratio estimate (1.5) results in a marginally significant *P* value (0.07).

ZIKV infection results in higher viral load and reduced body weight in undernourished pregnant mice

To experimentally investigate the relationship between protein malnutrition and CZS, we used wild-type C57BL/6 females. These were either maintained on a standard mouse diet (Co) or shifted to a low-protein diet (LP) 7 to 10 days before mating and throughout gestation. At embryonic day 12 (E12), dams were injected intraperitoneally with 10^6 plaque-forming units (PFU) of Brazilian ZIKV or the supernatant of noninfected *Aedes albopictus* C6/36 cells, Mock (Fig. 1C). Dams did not differ significantly in body weight by E12, but LP mothers at 3 days post-infection (dpi) showed significantly less weight in comparison to control diet groups (table S4 and Fig. 1D). In particular, LP/ZIKV dams had significantly less body weight than Co/Mock and Co/ZIKV ($P < 0.01$), while LP/Mock significantly differed from Co/ZIKV ($P < 0.05$) (Fig. 1D). To confirm protein undernutrition, we measured levels of leptin and insulin-like growth factor 1 (IGF1) in maternal serum at E15 through enzyme-linked immunosorbent assays (ELISAs). As expected, both hormones showed significantly lower levels in LP than in control diet groups (Fig. 1, E and F). To measure the maternal viral load, we processed spleen samples from the different groups and performed reverse transcription quantitative polymerase chain reaction (RT-qPCR) 3 dpi (Fig. 1G). LP/ZIKV maternal spleens showed increased viral load 3 dpi, while the virus was not detected in Co/ZIKV.

The placenta is affected after ZIKV and protein restriction exposure

As recent *in vivo* studies have shown that embryonic growth impairment could be at least partly explained by the placental injury (6, 19–21), we examined some aspects of this organ in our mouse model at E15 (Fig. 2). Both infected groups displayed a similar proportion of placentas with detectable viral RNA by RT-qPCR (Fig. 2B and fig. S3). ZIKV in the placental tissue was also localized using

anti-nonstructural protein 1 (NS1) and anti-double-stranded RNA (dsRNA) (J2) antibodies. NS1 is present in both Co/ZIKV and LP/ZIKV placentas, similar to the RT-qPCR analyses, although the ZIKV labeling is stronger in LP/ZIKV (fig. S4). Moreover, in LP/ZIKV placentas, J2-positive cells are colabeled with isolectin B4 (IB4), a marker of endothelial cells that, specifically in the placenta, reacts to labyrinth epithelial cells (fig. S5). In addition, negative strand-specific RT-qPCR assays were performed to quantify detectable replicative intermediate negative-strand RNA differences among the LP/ZIKV and Co/ZIKV groups. We found that LP/ZIKV placentas had a higher amount of negative-strand RNA than Co/ZIKV (fig. S5). Together, these results suggest that viral replication is higher in the placentas of the undernourished animals compared to control diet group.

At E15, some placentas showed abnormal labyrinth architecture: in the same blood space, both anucleated maternal red blood cells (RBCs) and nucleated embryonic RBCs were found (Fig. 2, A and C). This sign of vasculature damage was found in all the LP/ZIKV placentas ($n = 9$) and in a small portion (two placentas) of the total Co/ZIKV ($n = 8$), while it was absent both in Co/Mock ($n = 5$) and LP/Mock ($n = 5$). Furthermore, conspicuous areas of necrosis in the labyrinth were found in 55.5% of LP/ZIKV placentas (Fig. 2D). This histopathological feature was absent in the other groups (fig. S6). Last, we also found, in 44.4% of the LP/ZIKV placentas, hemorrhagic areas in the labyrinth, as illustrated in Fig. 2D. Together, cellular and molecular placental changes in LP/ZIKV indicate that a differential response is triggered in females when the effect of protein restriction diet and ZIKV infection are combined.

Embryonic body growth and neurogenesis is compromised by the interaction of protein malnutrition and ZIKV infection

The foregoing data demonstrate that maternal malnutrition associated with ZIKV infection impairs the placental structure. To determine whether the offspring development is affected in this context, we first analyzed morphological outcomes in embryonic life (E15). No significant differences were found in the size of the litters or the sporadic embryonic reabsorptions. As expected, we found that body weight at E15 is not compromised in noninfected LP pups (Fig. 3A). It is known that maternal protein undernutrition affects pup body weight only in later life (22). In contrast, ZIKV infection in the LP group results in a significant difference compared to the Co/Mock group (Fig. 3A). The body weight variance of LP/ZIKV displays a bimodal pattern, in which approximately half of the specimens showed growth restriction (Fig. 3A), statistically different when compared with the other groups ($P < 0.001$).

In addition to general growth restriction, we analyzed the viral load and morphological abnormalities in the E15 and E18 brains. RT-qPCR analysis of embryonic E15 brains revealed that both Co/ZIKV and LP/ZIKV have detectable viral load (fig. S7). At E18, brains from Co/ZIKV and LP/ZIKV displayed comparable viral loads, although two LP/ZIKV specimens from the same litter presented higher ZIKV RNA levels than Co/ZIKV (fig. S7). Using immunocytochemistry, we found colocalization of NS1⁺ cells with microglial ionized calcium-binding adapter molecule 1 (Iba1⁺) cells and endothelial CD31⁺ cells in the E15 brain both of Co/ZIKV and LP/ZIKV (figs. S8 and S9). However, abundant macrophage/microglia cells (Iba1⁺ cells) were found especially in the lateral ventricles of the LP/ZIKV group (Fig. 3B), reflecting a local response to congenital infection. ZIKV-infected cells (J2⁺) are found in LP/ZIKV specimens colocalized with IB4⁺ cells, a marker of endothelial and microglial cells in the brain (23) within the ventricular

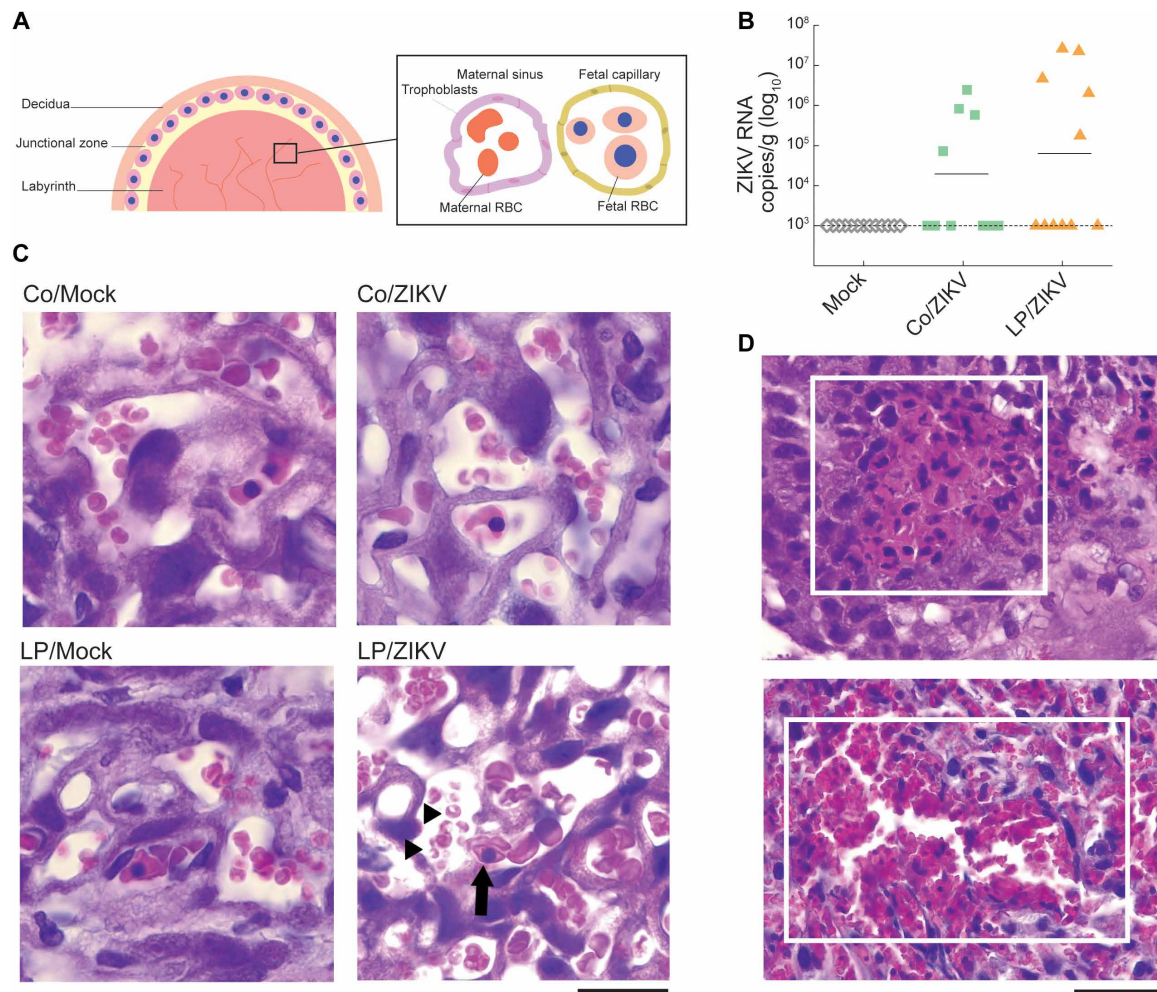


Fig. 2. Placental alterations 3 days after ZIKV infection in LP group. (A) Schematic representation of a placental structure. Normal labyrinth structure is characterized by separate maternal sinus with anucleated erythrocytes and embryonic capillaries with nucleated blood cells. (B) Viral load in the placentas was quantified by RT-qPCR (n per group E15: Mock = 13; Co/ZIKV = 10; and LP/ZIKV = 11; placentas were derived from five independent litters in each group). Lines indicate the geometric mean. Detectable viral RNA was found in 40% of Co/ZIKV placenta and in ~50% of LP/ZIKV placentas. No statistically significant difference in the amount of viral RNA was detected between means of Co/ZIKV and LP/ZIKV ($P > 0.05$). (C) Analysis of placental sections with hematoxylin and eosin (H&E) staining. Representation of altered labyrinth morphology with nucleated (embryonic, arrow) and anucleated (maternal, arrowheads) blood cells sharing the same vascular spaces found in LP/ZIKV placentas is shown. Scale bar, 20 μ m. (D) Necrotic areas were identified in the spongiotrophoblast of some LP/ZIKV cases (top), with abundant examples of pyknosis and karyorrhexis, suggesting the occurrence of this degenerative process. In addition, an example of the hemorrhagic area found in the LP/ZIKV labyrinth is shown (bottom). White frames were used to indicate the location of the lesion. Scale bar, 50 μ m.

zone (fig. S10). The ventricular and subventricular zones are also known as the proliferative zone in the developing cerebral cortex. To address whether maternal malnutrition and ZIKV infection affect neurogenesis, we examine proliferation with an antibody against anti-Ki67 to identify progenitors that were in any phase of the replicative cycle. These cycling progenitors (Ki67⁺) in the cortical proliferative zone of E15 were reduced in the LP/ZIKV experimental group in comparison to the other groups (Fig. 3C). Accordingly, the early-born infragranular neurons [as identified by COUP-TF-interacting protein 2 (CTIP2) antibody], which will occupy the layer V in the postnatal cortex, were also reduced in the developing cortical plate (Fig. 3D).

ZIKV infection modulates gene expression in the developing brain of malnourished pups

To determine the differential gene expression related to the described embryonic phenotypes, we performed RNA-seq analyses in

E15 brains. The combination of protein restriction and ZIKV produced large deregulation, particularly in genes involved in cell cycle control, mitotic progression, and neural development (Fig. 4A). Using a Circos plot analysis, we found 60 key clusters, indicating that a small number of hub genes deregulate a large number of genes in CZS (Fig. 4B). A critical pathway in neural stem cell proliferation, neuron differentiation and assembly, and maintenance of neural circuits, the mammalian target of rapamycin (mTOR) signaling pathway, is deregulated in LP/ZIKV (fig. S11). Beyond changes of entire pathways, specific key genes exhibited interesting patterns. For instance, genes related to neural development—such as *Ncam2*, *Shank1*, and *Icam5*—were down-regulated in LP/ZIKV (Fig. 4C). Moreover, *Kir3dl2*, a receptor located at the surface of natural killer cells and *Cd46*, which participates in T cell activation, were also down-regulated in LP/ZIKV (Fig. 4C). In contrast, we found important genes involved in antiviral (e.g., *Rps3* and *Ccr1*) and inflammatory

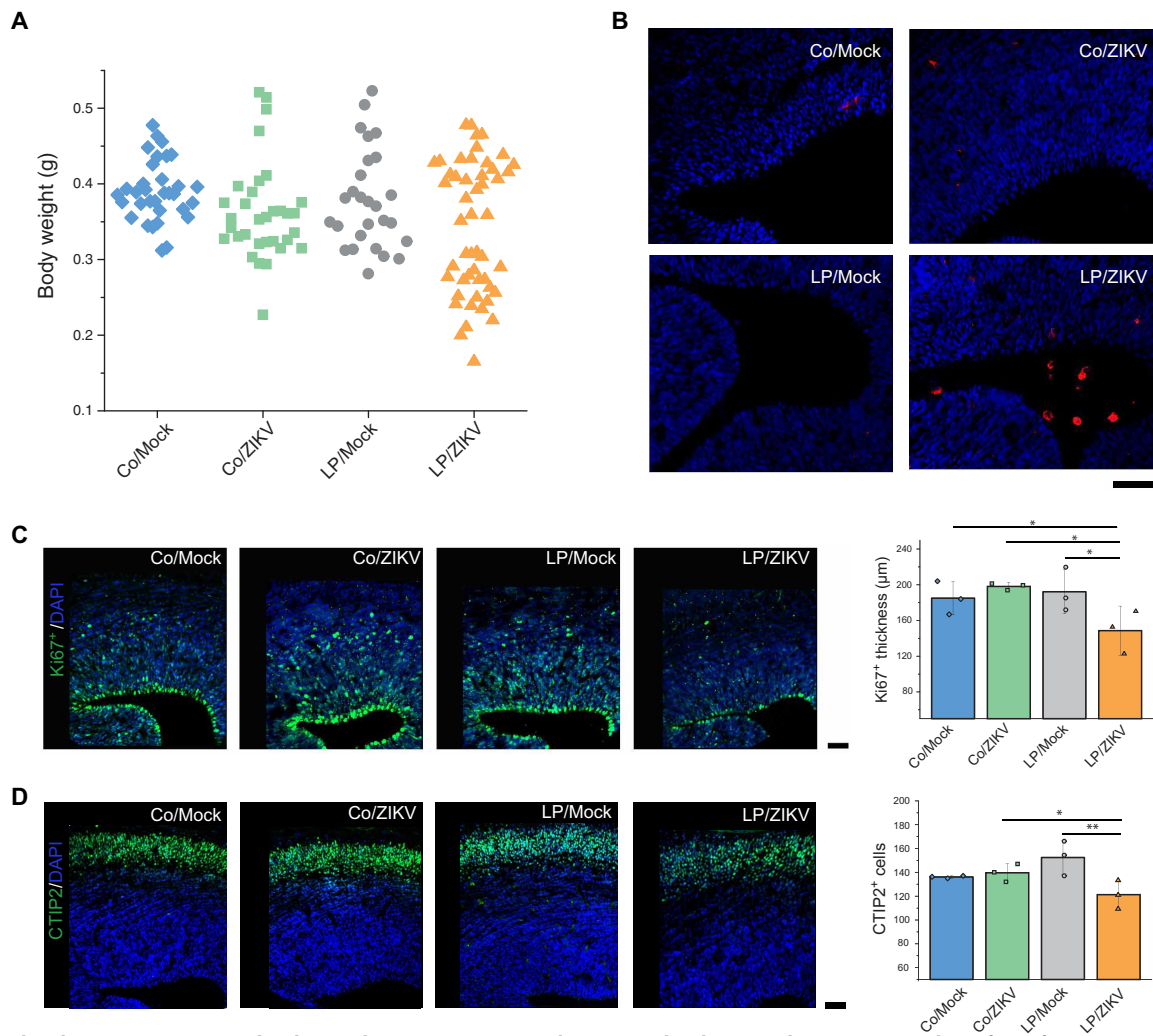


Fig. 3. Maternal undernutrition associated with ZIKV during pregnancy results in neurodevelopmental impairments 3 days after infection (E15). (A) Quantification of body weight of embryos at E15 [Kruskal-Wallis, 8.360 (*); multiple comparisons with Mann-Whitney *U*: Co/Mock versus LP/ZIKV, $Z = -1.959$ (*)]. Variance is significantly different between groups, as estimated by Bartlett test *K*-squared, 19.929 (***). (B) Analysis of microglia/macrophage recruitment with Iba1⁺ immunostaining (red) reveals the presence of reactive cells in the developing brain of LP/ZIKV group, in particular, in the lateral ventricles. (C) Immunostaining and quantification of cycling cells in the proliferative zone show a reduction of Ki67⁺ cells (green) in LP/ZIKV cortex. Analysis of variance (ANOVA) $F = 3.838$ (*); least significant difference (LSD): Co/Mock versus LP/ZIKV (*) (P -adj > 0.05), Co/ZIKV versus LP/ZIKV (*) (P -adj > 0.05), LP/Mock versus LP/ZIKV (*) (P -adj > 0.05), $df = 3$. DAPI, 4'-6-diamidino-2-phenylindole. (D) Immunostaining and quantification of early-born neurons labeled with CTIP2⁺ (green). LP/ZIKV results in a reduction in cortical neurons compared with controls. ANOVA $F = 4.77$ (*); LSD: Co/ZIKV versus LP/ZIKV (*) (P -adj > 0.05), LP/Mock versus LP/ZIKV (**) [P -adj < 0.05 (**)], $df = 3$ ($n = 3$ per each group; in all cases, three sections of each brain were quantified and averaged). * $P < 0.05$ and ** $P < 0.01$. The error bar represents mean \pm SD. Scale bars, 50 μ m.

response (e.g., *Il16* and *C1qtnf9*) that were up-regulated in LP/ZIKV, as well as genes that modulate apoptotic mechanisms, such as *Cdk1* and *Plk1* (Fig. 4D).

Neonates from undernourished and infected dams have reduced brain size

To understand whether those changes observed during embryonic life result in postnatal differences compatible with phenotypes described in CZS, we investigated postnatal offspring growth (Fig. 5). In neonates, body weight was significantly reduced in LP/ZIKV (Fig. 5C), while brain size was also impaired (Fig. 5, A, B, and D). Brains reconstructed using micro-computed tomography (μ CT) revealed the microcephaly phenotype-like only in the LP/ZIKV litters (Fig. 5A). Cerebral cortex sections counterstained with DAPI (4'-6-diamidino-

2-phenylindole) showed a reduction in the correspondent cortical wall area of this group when compared with the other controls (Fig. 5B). We found that LP/ZIKV brains were significantly smaller than those of the other groups (Fig. 5D). Since body weight and brain size are affected in LP/ZIKV, we examined whether brain size in this group corresponds to that expected for its body size. Using a linear regression between brain size and body weight, negative residuals were obtained for LP/ZIKV, indicating that brain size is relatively more affected than body weight in this group (fig. S12). In addition, morphometric analyses revealed that the cortical size is relatively more affected than the other brain areas in the LP/ZIKV group (Fig. 5E). We also assessed differences in skull size and found that LP/ZIKV specimens exhibited craniofacial growth impairment (fig. S13).

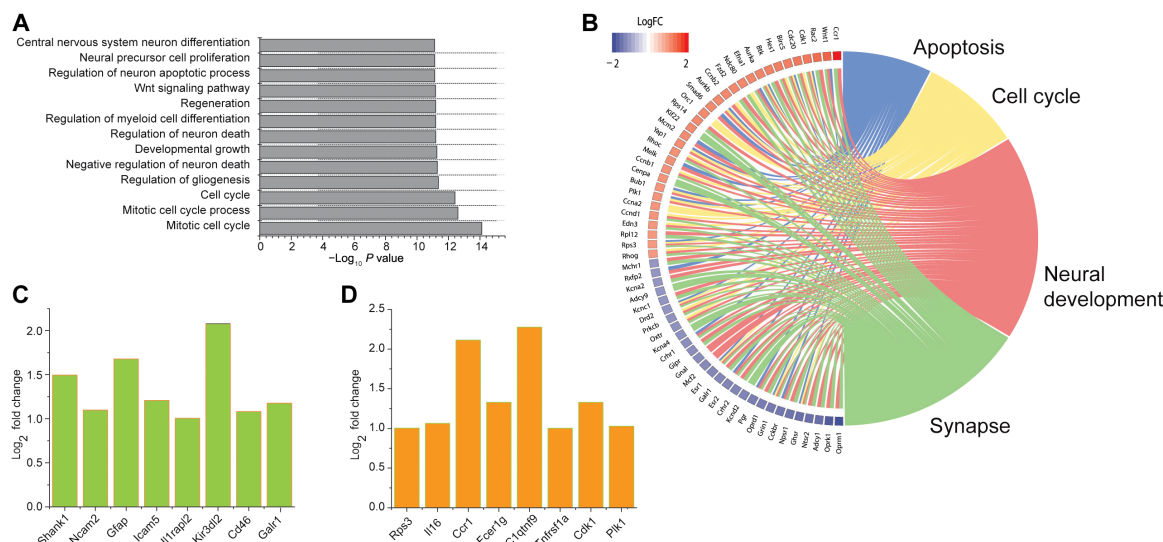


Fig. 4. LP and congenital ZIKV infection induce gene expression deregulation in embryonic brains. (A) Pathways reflecting biological processes that are deregulated in the LP/ZIKV in comparison to Co/ZIKV after RNA-seq analyses. Only those with large significant differences are presented. (B) Circos plot showing the 60 hub genes, most (red) and least (blue) expressed in LP/ZIKV (in comparison to Co/ZIKV) shared between relevant cellular processes. Individual selected genes that are significantly down-regulated (C) or up-regulated (D) in LP/ZIKV in comparison to Co/ZIKV. FC, fold change.

DISCUSSION

Although ZIKV is only responsible for mild symptoms in most adult cases, the recent experience in the Americas has alarmed the biomedical community because of a sudden increase in congenital abnormalities caused by this viral infection. Since CZS is distributed heterogeneously, cofactors could play a role in this asymmetrical pattern (9). Recently, it was suggested that fetal genetic background could predispose to malformation development after ZIKV vertical transmission (8). Beyond genetic predisposition, it was shown that environmental factors, such as the previous exposure to dengue virus, increase susceptibility to ZIKV congenital infection and lead to more exacerbated phenotypic alterations in the brain (24). Since immune status also depends on nutritional conditions, these are crucial elements to understand differential infection outcomes (13). Here, we identify the effect of nutritional restriction on CZS development.

First, we found that there is a positive correlation between regions with a high index of undernourished patients and regions with a high incidence of microcephaly cases registered during the ZIKV outbreak in Brazil. Furthermore, we interviewed mothers of CZS children and observed a reduced protein intake in approximately 40% of them. In comparison to the state and regional protein intake average, CZS mothers show a significant protein restriction. Moreover, the values obtained in our sample of CZS mothers differ from previously published references for pregnancies in other regions of Brazil (16–18). It has been reported that CZS is more prevalent in low-income populations (9, 11). Nutritional impairment has been found to result in the compromise of several innate and adaptive pathways of the immune system (25–28). Mainly, protein restriction is an issue in those vulnerable populations with limited access to more expensive food components (14). Together, on the basis of our data and previous studies, we propose that nutritional status could, at least partially, contribute to the asymmetrical prevalence of CZS.

The link between malnutrition and CZS was further investigated in vivo with wild-type mice (fig. S14). Different reports have found that adult wild-type mice under normal conditions are not very efficient

in replicating and vertically transmitting ZIKV (6, 29), and consequently, a large part of the research modeling ZIKV infection in vivo used immunocompromised animals (6, 19, 29, 30). Although vertical transmission of ZIKV is detected in some wild-type mice, these animals do not model the primary microcephaly associated with ZIKV infection (31), suggesting that disparities among models might depend on the particularities of the experimental designs such as ZIKV virus strain, amount of inoculated PFUs, and time between inoculation and harvesting, among others. Here, immunocompetent mice were used, allowing us to explore CZS in a context that better reflect pathophysiological responses in humans. We found that wild-type female mice exposed to protein restriction exhibit an increased viral load in the maternal spleens 3 days after infection. Previous work has also shown that adult wild-type C57BL/6J females infected with ZIKV intraperitoneally are capable of clearing the circulating virus in the first dpi (32). These results indicate that LP animals did not eliminate the circulating virus as soon as well-nourished animals, suggesting that antiviral response may be compromised in malnutrition. Differences in the maternal response to viral infection between Co/ZIKV and LP/ZIKV could reflect variations in the immunological maternal status, which might have an impact in the developing embryos. It has been described that ZIKV preferably replicates at the placenta (21). In our study, placentas from both infected groups (LP/ZIKV and Co/ZIKV) had comparable viral loads for total RNA detections, as measured by RT-qPCR. However, immunohistochemistry labeling using anti-J2 (dsRNA) and anti-NS1 antibodies as well as PCR analyses on replicative intermediate negative-strand RNA suggest that there are differences regarding viral replication of ZIKV between Co and LP infected groups.

Placental damage caused by ZIKV has been proven to be an important contributor to embryonic and fetal growth restriction (6, 19–21). Vasculature damage signatures in the placenta of malnourished and infected cases are comparable to what is described in other in vivo models of ZIKV vertical transmission (19, 33). Moreover, necrotic areas found in the labyrinth reflect severe pathological processes

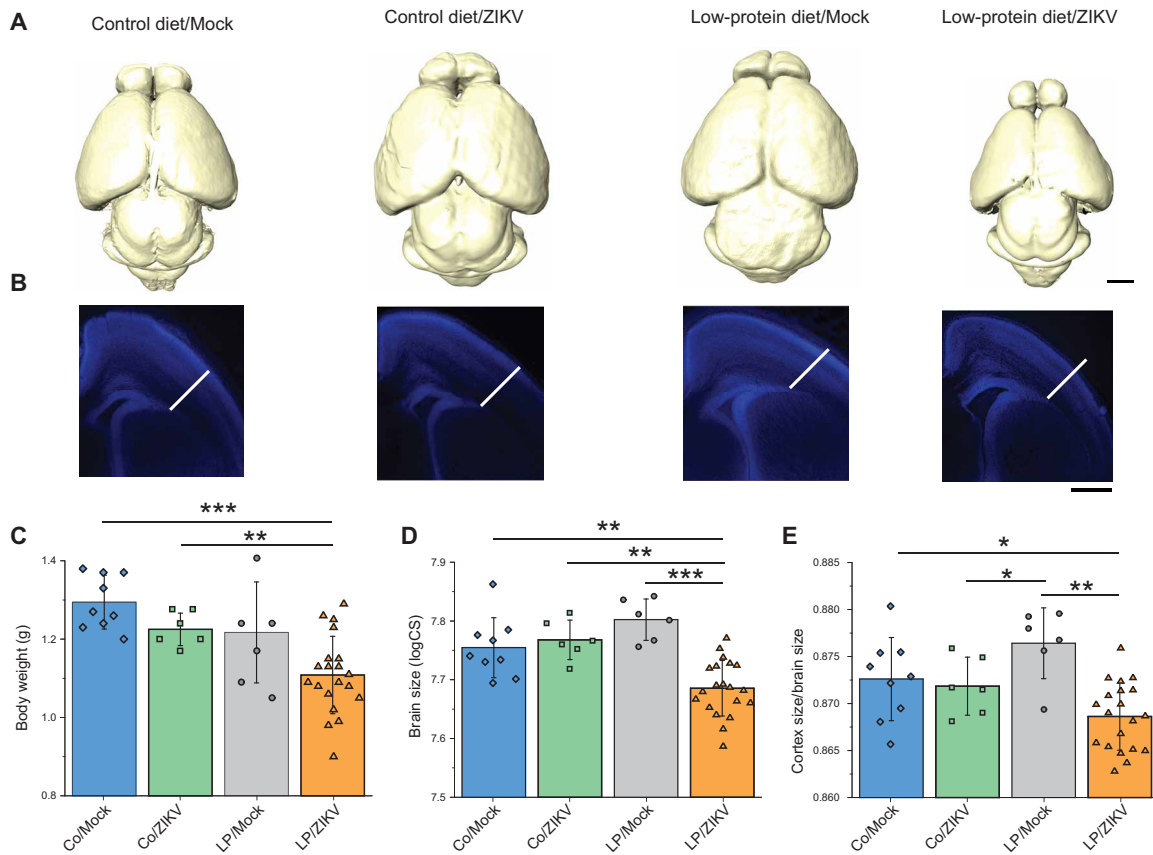


Fig. 5. LP mediates brain size reduction after ZIKV. (A) Representative three-dimensional reconstructions of brain anatomy of neonates obtained from μ CT illustrate size reduction in the LP/ZIKV group. Scale bar, 1 mm. (B) Coronal histological DAPI-stained sections also illustrate a cortical wall reduction (scale bar, 0.25 mm). The white measurement indicates the cortex thickness in the Co/Mock group, illustrated with the same size in all the other groups for comparative purposes. (C) Quantification of total body weight of newborns shows a significant decrease in the LP/ZIKV weight at P0. Kruskal-Wallis, 17.217 (***); multiple comparisons with Mann-Whitney *U*: Co/Mock versus Co/ZIKV, $Z = -1.724$; Co/Mock versus LP/Mock, $Z = -1.328$; Co/Mock versus LP/ZIKV, $Z = -3.634$ (***); Co/ZIKV versus LP/Mock, $Z = -0.216$; Co/ZIKV versus LP/ZIKV, $Z = -2.621$ (**); and LP/Mock versus LP/ZIKV, $Z = -1.857$. (D) Brain centroid size (CS), the square root of the summed squared distances of all digitized points to the centroid of the configuration, was obtained after the digitization of the three-dimensional position of 57 anatomical points. Kruskal-Wallis, 22.541 (***); multiple comparisons with Mann-Whitney *U*: Co/Mock versus Co/ZIKV, $Z = -0.707$; Co/Mock versus LP/Mock, $Z = -1.768$; Co/Mock versus LP/ZIKV, $Z = -3.158$ (**); Co/ZIKV versus LP/Mock, $Z = -1.609$; Co/ZIKV versus LP/ZIKV, $Z = -2.982$ (**); and LP/Mock versus LP/ZIKV, $Z = -3.530$ (***). (E) The proportion of cortex centroid size in relation to total brain centroid size. This proportion in LP/ZIKV group is smaller than in undernourished pups that have not been infected with ZIKV. Kruskal-Wallis, 13.743 (**); multiple comparisons with Mann-Whitney *U*: Co/Mock versus Co/ZIKV, $Z = -0.354$; Co/Mock versus LP/Mock, $Z = -1.768$; Co/Mock versus LP/ZIKV, $Z = -2.216$ (*); Co/ZIKV versus LP/Mock, $Z = -2.082$ (*); Co/ZIKV versus LP/ZIKV, $Z = -1.765$; and LP/Mock versus LP/ZIKV, $Z = -3.043$ (**). * $P < 0.05$, ** $P < 0.01$, *** $P < 0.001$, and $P > 0.05$. The error bars represent means \pm SD.

occurring in this organ. Analysis of the LP/ZIKV placenta indicates that a differential local response is triggered at E15, shortly after the infection, at E12, with concomitant structural alterations. In contrast, immunocompetent dams infected with ZIKV earlier, at E9.5, also display structural placental damage after 4 dpi (21). Thus, these results point out that the severity of the placental impairment resulting from ZIKV infection depends on the embryonic stage of infection and the harvesting time point. This placental damage could be essential to understand some features of growth impairment in the offspring that not only result from direct embryonic infection but also indirect pathogenic mechanisms. In sum, we agree on the importance of placental insufficiency effects in the emergence of CZS beyond direct fetal infection (19–21).

Associated with a differential maternal response to ZIKV infection and placental damage, we found phenotypic changes in the LP infected group comparable to previous descriptions of CZS both in humans and in animal models: intrauterine growth re-

striction, placental injury, impaired neurogenesis, and local inflammation (5, 7, 34). Body weight reduction is a clear sign of intrauterine growth restriction, a condition that was described as part of CZS in humans (7, 34, 35) and mouse models (5, 6). Recently, a survey showed that the prevalence of low birth weight is four times higher in CZS children compared to other newborns from the same region (36). In our assays, we found body weight reduction in infected malnourished litters, consistent with the findings in human CZS cases. A recent study on wild-type C57BL/6J mice have found that vertical transmission of ZIKV after intraperitoneal injection on pregnant females does not result in morphological alterations in the offspring during perinatal life but negative outcomes appeared later in postnatal life (31). This coincides with our results of Co/ZIKV in which we confirmed ZIKV congenital infection, but we did not find phenotypic signals of CZS in embryos and neonates. Since structural alterations were found here during prenatal and early postnatal life in the LP/ZIKV group, these results suggest that protein restriction diet

contributes to the negative outcomes on ZIKV congenitally infected specimens.

The devastating consequences of ZIKV infection in developing nervous systems were previously linked to its tropism for immature neural cells (3). Here, embryonic macrophagic cells in the brain co-localized with ZIKV. A previous *in vitro* study showed that microglia cells are also a ZIKV target (37). Thus, neuroinflammation could play a key role in the pathogenesis of CZS. In this neuropathological context, we described impairment of the neurogenesis and cortical development pre- and postnatally. The cerebral cortex is relatively more affected in LP/ZIKV than other brain structures, similar to what is described in human CZS (34). To molecularly understand those effects on brain development associated with malnutrition and ZIKV infection, we performed RNA-seq. Comparing the group where infection was combined with nutritional restriction, the control diet infected animals resulted in altered molecular pathways related to cell cycle, viral replication, DNA damage, and inhibition of neurogenesis. This largely coincides with those deregulated pathways in the 3-day *in vitro* ZIKV-infected neurospheres (4). More specifically, because of ZIKV infection following undernutrition, some genes, such as *Cd46*, relevant to immune response are down-regulated, and proinflammatory response genes, such as *Il6*, are up-regulated. Several genes required for normal brain development, like *Shank1* and *Ncam2*, are down-regulated in LP/ZIKV, indicating that specific processes leading to neural growth and patterning are impaired. Besides, the mTOR signaling pathway, significant for neural development, is deregulated. Similarly, a previous report also found alterations of this pathway in CZS human twins (8).

Malnutrition is one of the most frequent causes of increased susceptibility to infectious disease (12, 13) and is a widespread problem in low-income populations (38). Our experimental approach provides a framework for investigating the interaction of malnutrition and ZIKV *in vivo*. We have found that protein restriction mediates ZIKV infection and exacerbates developmental impairment in the offspring, suggesting that the nutritional status of the dam can be a determining factor in differential susceptibility to CZS. ZIKV infection is a complex pathological process in which the magnitude of the congenital abnormalities is not only associated with the viral load in each tissue; indirect factors such as placental damage can also play important roles in development of these abnormalities (19, 21). To deepen current knowledge on the emergence of CZS, it is essential to understand the cofactors modulating previous outbreaks, thus improving preventive measurements facing future epidemics.

MATERIALS AND METHODS

Epidemiological analyses on Brazilian cases of microcephaly and undernutrition

First, data were obtained from the Brazilian Ministry of Health via the integrated data bank RESP (Registro de Eventos em Saúde Pública/Public Health Events Registry) to quantify the total amount of cases of microcephaly that were confirmed and reported still under examination between 2015 and 2018. This amount was standardized by 1000 inhabitants. The total number of patients hospitalized by any type of undernutrition between 2009 and 2018, normalized by 1000 inhabitants, were extracted from the Brazilian Ministry of Health public data bank CID-10 (Classificação Estatística Internacional de Doenças e Problemas Relacionados à Saúde/International Statistical Classification of Diseases and Related Health

Problems) available at www.datasus.gov.br/cid10/V2008/cid10.htm. Undernutrition was defined by the health agents as cases diagnosed and satisfying at least one of the following conditions: kwashiorkor, nutritional marasmus, severe calorie-protein undernutrition, moderate to mild calorie-protein undernutrition, growth retardation due to calorie-protein undernutrition, and nonspecified calorie-protein undernutrition. For the definition of these categories, which were codified as E40-46 in the CID-10 public bank, the criteria defined by the World Health Organization were applied. A decade's worth of data regarding hospitalization due to undernutrition was taken to have a more consistent description of this variable. The coefficient of variation for the raw number of patients hospitalized by undernutrition over these years ranged between 2.00 for the state of Sergipe and 11.15 for the state of Espírito Santo. To avoid sampling bias, municipalities with less than 20,000 inhabitants were excluded. Values for both variables (microcephaly and undernourishment) were obtained for all tropical states in the Northeast, North, Central-West, and Southeast regions. A Pearson correlation analysis was performed, and a simple linear regression was also carried out to assess the association between both variables. After obtaining a *P* value under the assumptions of a parametric test for this correlation, a simulation approach was used to estimate the significance of the correlation using a Monte Carlo permutation analysis. For this purpose, the values from our original sample were randomly correlated (999 times), and the frequency of each *r* coefficient was registered and illustrated in fig. S1. Then, by comparing our original *r* coefficient in the simulated distribution, it was possible to detect how probable our correlation to occur by chance is, and an adjusted *P* value was derived.

In addition, a survey on a sample of mothers who have children with CZS was performed in the Northeastern state of Ceará. We interviewed 83 affected mothers, and a diet frequency questionnaire was completed, in which we asked the number of times they ate different categories of foods per week. Data that support this part of the study are available on request from the corresponding author (P.P.G.). Ethical approval was obtained for data collection in protocol 2385592 from the Federal University of Ceará. On this basis, we quantified the amount of daily protein consumption by multiplying the daily frequency of consumption of each food by the protein content of this food in a standard portion. The total daily protein intake was obtained by summing these values for the consumed foods, as described by Rogers and Emmett (39). According to current recommendations, the average consumption of protein during pregnancy should be above ~60 g/day (www.nrv.gov.au/nutrients/protein). We subsequently quantified the number of cases where consumption was either below or above 61 g/day to have an estimation of the portion of the sample affected by low protein intake.

The pattern of protein intake obtained from the interviewed mothers was compared with a reference for the state of Ceará and the whole Northeast region. For this purpose, we used the "Survey of familiar incomes 2008-2009" (Pesquisa de orçamento familiares 2008-2009) database of the IBGE and depicted the average values for Ceará and the Northeast together with the histogram of our sample. For Ceará state, the average value of protein intake was estimated from the data on the frequency of consumption of different foods, while the value of daily protein intake for the entire Northeastern region is available in the IBGE data bank by age and sex. In this case, the protein intake of women between 19 and 59 years was taken as a reference. In addition, we statistically compared the means of our sample and reference of Ceará for the variable daily

protein intake using a *t* test. Similarly, we estimated the relative risk of CZS in relation to the protein intake level. Since our condition (CZS) had low frequency in the population, we carried out the analyses under “the rare disease assumption” and estimated the odd ratio (40). Given that the frequency of CZS is rare in the population, reference data for Ceará can be considered as representative of the protein intake of a non-CZS group.

Experimental design: Diet and infection

C57BL/6 nulliparous female 6-week-old mice were obtained from the Animal Care Facility of the Microbiology Institute of the Federal University of Rio de Janeiro. They were divided into two groups according to the consumed diet. Control females were fed a standard diet with the recommended amount of macro- and micronutrients (TD91352, Harlan Teklad, Madison). In the control diet, protein content was 20.3%. In contrast, the LP group received a diet with 6.1% of protein in the form of casein and DL-methionine. These diets are isocaloric (3.8 kcal/g), having the same percentage of fat (5.5%) and a different proportion of carbohydrates (control, 61.6%; LP, 75.6%).

Administration of both diets started 7 to 10 days before mating and continued until the harvesting dates. Animals had ad libitum access to water and food. Throughout the whole experiment, we assessed food intake daily. No significant differences between groups were found regarding the amount of consumed food. Females were housed in single cages throughout the whole experiment. Pregnancy was confirmed through observation of the postcoital vaginal plug to have an accurate estimation of embryonic age.

On E12, we performed intraperitoneal injections in control and LP dams of ZIKV (infected) or Mock (noninfected). Dams were injected with 10^6 PFU of a Brazilian ZIKV strain obtained from a patient presenting typical symptoms of ZIKV infection (Recife/Brazil, ZIKV PE/243, accession no. KX197192.1) (41). For experimental comparisons with noninfected animals, we injected control and LP dams with the supernatant of *A. albopictus* C6/36 cells (Mock). The viral titer of the stock was 3.4×10^6 PFU/ml, and the injected volume was 295 μ l. These treatments yielded four experimental groups: control/Mock (control diet, noninfected), control/ZIKV (control diet, ZIKV infected), LP/Mock (LP, noninfected), and LP/ZIKV (LP/ZIKV infected). Harvesting of samples was carried out during embryonic life in E15 and on the first day of postnatal life (P0). In the case of E15 sample harvesting, dams were culled using cervical dislocation. Neonates at P0 were decapitated. Embryos and neonates were weighed on a standard laboratory scale with a definition of 1 mg (OHAUS, USA) before decapitation.

Weight in E15 embryos was measured in specimens of each litter giving a total sample of $n = 33$ (Co/Mock), $n = 33$ (Co/ZIKV), $n = 27$ (LP/Mock), and $n = 50$ (LP/ZIKV). For Co/Mock, five independent litters in E15 were used (number of embryos for each litter = 3, 7, 7, 8, and 8), while for the Co/ZIKV embryos, weights derived from six independent litters (number of embryos for each litter = 2, 3, 5, 6, 8, and 9) were measured. For LP/Mock, four independent litters were used (number of embryos for each litter = 5, 7, 7, and 8), and last, in LP/ZIKV, embryos from seven litters were weighed (number of embryos for each litter = 5, 6, 6, 6, 8, 9, and 10). In P0, we reported body weights from those specimens that were CT-scanned to obtain brain size (Co/Mock, $n = 9$ neonates from three independent litters; Co/ZIKV, $n = 6$ neonates from two independent litters; LP/Mock, $n = 6$ neonates from three independent litters; and LP/ZIKV, $n = 20$ from four independent litters).

ZIKV was propagated in C6/36 cells. Briefly, C6/36 cells were infected at a multiplicity of infection of 0.01 and incubated at 37°C. After 1 hour, the inoculum was removed and replaced with growth media supplemented with 2% fetal bovine serum. After 6 days, the conditioned medium was harvested, centrifuged at 300g, and filtered through 0.22 μ m to remove cells and cellular debris. Supernatants were collected and stored at -80°C . Virus titers were determined by plaque assay performed on Vero cells.

All animals used in this study were housed in the Animal Care Facility of the Microbiology Institute of the Federal University of Rio de Janeiro. All procedures were approved by institutional ethical committee, protocol CEUA-CCS/UFRJ 01200.001568/2013-87.

Viral detection

RNA was extracted from maternal spleen, placentas, and embryonic brains using the TissueRuptor (IKA) and the RNeasy Plus Mini Kit (QIAGEN), following the recommendations of the manufacturer. To quantify viral RNA, we used One Step TaqMan RT-qPCR (Thermo Fisher Scientific) on a 7500 Real-Time PCR System (Applied Biosystems) with primers and probe described by Lanciotti *et al.* (42). ZIKV copies were determined by interpolation onto a standard curve composed of eight 10-fold serial dilutions of a synthetic ZIKV RNA based on the Asian lineage. The ZIKV quantification was expressed as ZIKV RNA copies per gram of tissue. For maternal spleens 3 dpi, the sample size was 4 for Mock, 4 for Co/ZIKV, and 5 for LP/ZIKV. In addition, in E15 placentas, the sampling included organs from five independent litters for each group. Numbers of placentas of each litter within each group were as follows: Mock = 1, 1, 2, 3, and 6 ($n = 13$); Co/ZIKV = 1, 1, 2, 3, and 3 ($n = 10$); and LP/ZIKV = 2, 2, 2, and 3 ($n = 11$).

For the specific negative-strand RNA detection, total RNA from tissue samples was purified with the RNeasy Plus Mini Kit (QIAGEN), following the manufacturer's recommendations. Reverse transcription was performed with the High-Capacity cDNA Reverse Transcription Kit (Thermo Fisher Scientific) using only forward primers (ZIKV 1086) for the specific retrotranscription of the negative strand of viral RNA. Subsequently, qPCR was performed using the ZIKV PrimeTime assay (IDT) on the GoTaq Probe qPCR System (Promega). A standard curve provided by serial dilutions of ZIKV synthetic RNA was used for absolute quantification.

Measurements of hormones in maternal serum

Systemic levels of IGF1 and leptin were assessed in maternal serum using the following kits: Abcam ab100695 and a100718. The procedures were carried out according to the manufacturer's suggestions. In these analyses, serum from three to four dams of each group was analyzed at E15.

Immunostaining and imaging analyses of embryonic brain

Brains of E15 embryos were fixed with 4% paraformaldehyde (Sigma-Aldrich, USA) overnight and then embedded in 30% sucrose to provide cryoprotection to the tissue. Coronal sections (10 μ m) were obtained with a cryostat (Leica, Germany), permeabilized with 0.1% Triton X-100 (Sigma-Aldrich, USA), and incubated with 3% bovine serum albumin (Sigma-Aldrich, USA). After standard antigenic retrieval, the following primary antibodies were incubated overnight: mouse J2 anti-dsRNA I (1:500), rat anti-CTIP2 (1:500; Abcam, ab18465), rabbit anti-Ki67 (1:100; EMD Millipore, AB9260), mouse anti-Iba1 (1:200; EMD Millipore, MABN92), rabbit anti-Iba1 (1:500 Wako

Chemicals USA Inc.), and rabbit anti-CD31 (Abcam, ab28364). Subsequently, samples were washed with phosphate-buffered saline (PBS) and incubated with secondary antibodies: goat anti-mouse Alexa Fluor 488 (1:500; Abcam, ab150113), goat anti-rat Alexa Fluor 488 (1:500; Abcam, ab150157), and goat anti-mouse Alexa Fluor 546 (1:500; AP192SA6) (Thermo Fisher Scientific, USA). In those sections where IB4 (1:50; Vector Laboratories, FL1201) was used, it was incubated with secondary antibodies for 2 hours. Nuclei were stained with DAPI (0.5 µg/ml) for 20 min. Images were acquired with a TCS SP8 confocal microscope (Leica, Germany) and a laser scanning confocal microscope (Olympus FV1000, Japan) with 20×, 40×, or 63× objective high numerical apertures.

In all cases, at least three brains of each experimental group were examined and analyzed. Brains in each group belong at least to two different litters. For each brain, three consecutive sections were analyzed, and an average of their results was taken as the representative value for the specimen. All data collection was performed by one of the authors (J.B.-A.) using a blinding code. Previous to definite data collection, we analyzed intraobserver repeatability in a subsample of images and confirmed consistency in marker identification. Analyses of the acquired images were carried out using Fiji software (43). We performed a quantitative analysis based on the work by Wu *et al.* (32) where the band thickness of positive-stained cells was analyzed. Here, we measured the distance between the ventricular limit and the most upper located Ki67⁺ cells. For CTIP2 staining, we counted the absolute number of cells that were positive in an area with a height of 100 µm and a width of 70 µm.

Placenta histology

For hematoxylin and eosin (H&E) staining, placentas were embedded in paraffin blocks and sectioned at 5 µm after overnight fixation in 4% paraformaldehyde. On these sections, a qualitative observation was carried out to examine the general structure of decidua and labyrinth regions. Fluorescent staining on placentas was performed on frozen sections of 10 µm obtained from cryostat. Sections were prepared with the same protocol used for brain immunostaining and were incubated overnight with mouse anti-J2. After PBS wash, sections were incubated with goat anti-mouse Alexa Fluor 546 (1:500; AP192SA6) (Thermo Fisher Scientific, USA) and IB4, an isolectin for vasculature staining. In addition, we used a mouse anti-NS1 antibody (1:100; EA88) (Thermo Fisher Scientific, USA) to detect ZIKV in the placenta. Following incubation of the primary antibody, a goat anti-mouse Alexa Fluor 488 (1:1000, A28175) (Thermo Fisher Scientific, USA) was used.

Total RNA-seq

Total RNA was isolated from brains of E15 embryos using TRIzol (Invitrogen) protocol, followed by an analysis of quality with Bioanalyzer (Agilent) and quantity Qubit (Invitrogen). Subsequently, those samples were submitted to library construction using TruSeq Stranded mRNA HT Sample Prep Kit (Illumina), in which mRNA is enriched across magnetic beads with oligo(dT). This enriched mRNA template is converted to double-stranded cDNA, followed by AMPure XP bead purification, end repair, and A-tail addition. For each sample, an index was associated, and so, the library was amplified by PCR to enable cluster generation for sequencing at HiSeq 2500 (Illumina). The RNA-seq data were mapped to the Genome Reference Consortium Mouse Build 38 (GRCm38-mm10) with STAR 2.5.4b algorithm (44) after count tables for each gene was generated by HTSeq. The differ-

ential expression of genes was done in edgeR package. Gene Ontology enrichment analysis was performed with the R package GAGE 2.3. From the list of differentially expressed genes ($P < 0.05$ and log fold change, ≤ -1 or ≥ 1), we performed gene set enrichment analysis using ensemble of gene set enrichment analyses and derived a protein-protein interaction network with NetworkAnalyst.

A list of differentially expressed genes is available in table S5. For validation, five differentially expressed genes were selected from Fig. 4 (C and D) and analyzed by RT-qPCR (*Ccr1*, *Shank1*, *Galr1*, *Grin1*, and *Slc6a7*). For this purpose, purified RNA samples were submitted to retrotranscription followed by qPCR reaction in a one-step reaction protocol. The constitutive gene used was *GAPDH*, which showed good performance in mice in E15 (45). Results of relative expression were expressed by $2\Delta\Delta CT$. We used the GoTaq 1-Step RT-qPCR System (Promega) for *Ccr1* and *Shank1*, and for quantification of *Galr1*, *Grin1*, and *Slc6a7*, the LightCycler 480 System (Roche Life Sciences) was used. Results are presented in fig. S15.

µCT and morphometric analysis

µCT of the brains and skulls were performed at P0. Images were obtained using a Bruker SKYSCAN 1173 µCT scanner. To obtain skull images, neonates' heads were scanned following these parameters: isotropic voxel size of 8.19 µm, 30 kV, and 200 µA. For brains, we rescanned heads, but they were previously soaked for 24 hours in Lugol's iodine as a contrast agent following the work by Metscher (46). Scanning parameters for brain images with contrast were an isotropic voxel size of 8.19 µm, 50 kV, and 160 µA.

We used Amira software to build three-dimensional reconstructions and to register the position of anatomical points (landmarks). For skulls, a set of 42 bilateral landmarks was registered for each specimen, as described by Gonzalez *et al.* (fig. S13) (22). For brains, we followed the protocol proposed by Gonzalez *et al.* (22) to obtain the position of 57 landmarks and semilandmarks. Data collection was performed by one of the authors (J.B.-A.), who had previously applied the same protocol and measured the intraobserver error for this kind of data (22). Landmark and semilandmark coordinates were superimposed (Procrustes Analysis), and comprehensive measures of skull and brain size (centroid size) were obtained. Briefly, centroid size is defined as the square root of the summed squared distances of all digitized landmarks to the centroid of the configuration. Total brain size was estimated following this formula and using all the digitized points. In addition, since each point was digitized in an identifiable brain structure, for further analysis, we examined those landmarks and semilandmarks describing only the cortex. Figure S12 shows a transversal view of the cortex described by points 7 to 16, while in the sagittal, the cortex is represented by 16 to 23. Then, this restricted set of landmarks and semilandmarks describing the cortex was used to calculate cortex centroid size. A ratio between cortex and total brain centroid size was obtained for each experimental group as a variable to compare the proportion of the cortex in relation to the whole brain. Larger ratios correspond to brains in which cortex is relatively larger, while smaller ratios indicate that the cortex is relatively reduced.

While we did not digitize semilandmarks in the skull, in the brain, its structure demanded the use of semilandmarks (fig. S12). In this case, semilandmarks were sliced previously to superimposition using the function *procSym* of the Morpho R package.

The relationship between body weight and brain size was examined to understand whether the registered brain sizes correspond to the expected values for their body weights. For this purpose, a linear

model was carried out for the brain centroid size on body weight and the resulting residuals, which represent the deviations of the actual brain size of each case from the predicted value according to the body weight, as described by Gonzalez *et al.* (22). Positive values for the residuals indicate that brain size is larger than expected for certain body weight, while negative values suggest that brain size is smaller for body weight.

Statistical analyses

For all variables, a preliminary Kolmogorov-Smirnov test was carried out to test normality. Statistical analyses regarding comparisons between experimental groups were performed using analysis of variance (ANOVA), followed by a two-tailed least significant difference post hoc test with R, and a false discovery rate correction for multiple comparisons (47). Because of the distribution observed in the weight of E15 embryos, we performed a Bartlett test of homogeneity of variances using R as well. Before statistical analyses, we tested for power analysis according to our sample sizes by means of the function `pwr.anova.test` in R. For those variables that had at least one experimental group that departs from normality, we performed comparisons between means using the Kruskal-Wallis test, and in those cases in which significant difference was detected, we performed pairwise comparisons using Mann-Whitney *U* analyses. **P* < 0.05, ***P* < 0.01, and ****P* < 0.001.

SUPPLEMENTARY MATERIALS

Supplementary material for this article is available at <http://advances.sciencemag.org/cgi/content/full/6/2/eaaw6284/DC1>

Fig. S1. Distribution of simulated *r* coefficients for the correlation between undernutrition and microcephaly cases in tropical states of Brazil obtained after permutation of the original dataset.

Fig. S2. Number of ZIKV infection confirmed cases in each Brazilian state.

Fig. S3. Viral load in E18 placentas was quantified by RT-qPCR.

Fig. S4. Confirmation of ZIKV detection by immunohistochemistry in E15.

Fig. S5. Viral replication in LP/ZIKV placentas at E15.

Fig. S6. H&E staining in E15 placentas.

Fig. S7. Viral load in E15 and E18 embryonic brains quantified by RT-qPCR.

Fig. S8. ZIKV-infected cells colocalize with endothelial cells in E15 brains.

Fig. S9. ZIKV-infected cells colocalize with microglial cells in E15 brains.

Fig. S10. Staining of J2 on E15 embryonic brains colocalized with IB4.

Fig. S11. Network describing altered genes involved in the mTOR pathway.

Fig. S12. Morphometric analysis of brain images obtained through μ CT.

Fig. S13. Skull size of LP/ZIKV newborns is reduced.

Fig. S14. Summary of the results obtained with the experimental model.

Fig. S15. Validation of differentially expressed genes by RT-qPCR in E15 brains of Co/ZIKV and LP/ZIKV.

Table S1. Relationship between cases of undernutrition reported in hospitals and medical services and cases of microcephaly between 2015 and 2018.

Table S2. The estimated amount of daily protein (g) intake for each of the 83 interviewed mothers who have children with CZS.

Table S3. Relative risk of CZS in relation to protein intake.

Table S4. Maternal body weight (mean and SD) at the different pregnancy stages of the mouse model.

Table S5. Differentially expressed genes between Co/ZIKV and LP/ZIKV.

[View/request a protocol for this paper from Bio-protocol.](#)

REFERENCES AND NOTES

- W. K. de Oliveira, G. V. A. de França, E. H. Carmo, B. B. Duncan, R. de Souza Kuchenbecker, M. I. Schmidt, Infection-related microcephaly after the 2015 and 2016 Zika virus outbreaks in Brazil: A surveillance-based analysis. *Lancet* **390**, 861–870 (2017).
- H. Tang, C. Hammack, S. C. Ogden, Z. Wen, X. Qian, Y. Li, B. Yao, J. Shin, F. Zhang, E. M. Lee, K. M. Christian, R. A. Didier, P. Jin, H. Song, G.-L. Ming, Zika virus infects human cortical neural progenitors and attenuates their growth. *Cell Stem Cell* **18**, 587–590 (2016).
- P. P. Garcez, E. C. Loiola, R. Madeiro da Costa, L. M. Higa, P. Trindade, R. Delvecchio, J. M. Nascimento, R. Brindeiro, A. Tanuri, S. K. Rehen, Zika virus impairs growth in human neurospheres and brain organoids. *Science* **352**, 816–818 (2016).
- P. P. Garcez, J. M. Nascimento, J. M. de Vasconcelos, R. Madeiro da Costa, R. Delvecchio, P. Trindade, E. C. Loiola, L. M. Higa, J. S. Cassoli, G. Vitória, P. C. Sequeira, J. Sochacki, R. S. Aguiar, H. T. Fuzii, A. M. B. de Filippis, J. L. da Silva Gonçalves Vianez Júnior, A. Tanuri, D. Martins-de-Souza, S. K. Rehen, Zika virus disrupts molecular fingerprinting of human neurospheres. *Sci. Rep.* **7**, 40780 (2017).
- F. R. Cugola, I. R. Fernandes, F. B. Russo, B. C. Freitas, J. L. M. Dias, K. P. Guimarães, C. Benazzato, N. Almeida, G. C. Pignatari, S. Romero, C. M. Polonio, I. Cunha, C. L. Freitas, W. N. Brandão, C. Rossato, D. G. Andrade, D. d. P. Faria, A. T. Garcez, C. A. Buchpigiel, C. T. Braconi, E. Mendes, A. A. Sall, P. M. d. A. Zanotto, J. P. S. Peron, A. R. Muotri, P. C. B. Beltrão-Braga, The Brazilian Zika virus strain causes birth defects in experimental models. *Nature* **534**, 267–271 (2016).
- J. J. Miner, B. Cao, J. Govero, A. M. Smith, E. Fernandez, O. H. Cabrera, C. Garber, M. Noll, R. S. Klein, K. K. Noguchi, I. U. Mysorekar, M. S. Diamond, Zika virus infection during pregnancy in mice causes placental damage and fetal demise. *Cell* **165**, 1081–1091 (2016).
- P. Soares de Oliveira-Szejnfeld, D. Levine, A. S. d. O. Melo, M. M. R. Amorim, A. G. M. Batista, L. Chimelli, A. Tanuri, R. S. Aguiar, G. Malinger, R. Ximenes, R. Robertson, J. Szejnfeld, F. Tovar-Moll, Congenital brain abnormalities and Zika virus: What the radiologist can expect to see prenatally and postnatally. *Radiology* **281**, 203–218 (2016).
- L. C. Caires-Júnior, E. Goulart, U. S. Melo, B. H. S. Araujo, L. Alvizi, A. Soares-Schanoski, D. F. de Oliveira, G. S. Kobayashi, K. Griesi-Oliveira, C. M. Musso, M. S. Amaral, L. F. da Silva, R. M. Astray, S. F. Suárez-Patiño, D. C. Ventini, S. Gomes da Silva, G. L. Yamamoto, S. Ezquina, M. S. Naslavsky, K. A. Telles-Silva, K. Weinmann, V. van der Linden, H. van der Linden, J. R. M. de Oliveira, N. M. R. Arrais, A. Melo, T. Figueiredo, S. Santos, J. G. C. Meira, S. D. Passos, R. P. de Almeida, A. J. B. Bispo, E. A. Cavaleiro, J. Kalil, E. Cunha-Neto, H. Nakaya, R. Andreato-Santos, L. C. de Souza Ferreira, S. Verjovski-Almeida, P. L. Ho, M. R. Passos-Bueno, M. Zatz, Discordant congenital Zika syndrome twins show differential in vitro viral susceptibility of neural progenitor cells. *Nat. Commun.* **9**, 475 (2018).
- J. Barbeito-Andrés, L. Schuler-Faccini, P. P. Garcez, Why is congenital Zika syndrome asymmetrically distributed among human populations? *PLOS Biol.* **16**, e2006592 (2018).
- Instituto Brasileiro de Geografia e Estatística, *Indicadores Sociais da população brasileira* (Gerência de Biblioteca e Acervos Especiais, Rio de Janeiro, 2015).
- W. V. de Souza, M. d. F. P. M. de Albuquerque, E. Vazquez, L. C. A. Bezerra, A. da Cruz Gouveia Mendes, T. M. Lyra, T. V. B. de Araujo, A. L. S. de Oliveira, M. C. Braga, R. A. de Alencar Ximenes, D. de Barros Miranda-Filho, A. P. de Santana Cabral Silva, L. Rodrigues, C. M. T. Martelli, Microcephaly epidemic related to the Zika virus and living conditions in Recife, Northeast Brazil. *BMC Public Health* **18**, 130 (2018).
- P. Katona, J. Katona-Apte, The interaction between nutrition and infection. *Clin. Infect. Dis.* **46**, 1582–1588 (2008).
- J. Weger-Lucarelli, H. Auerswald, M. Vignuzzi, P. Dussart, E. A. Karlsson, Taking a bite out of nutrition and arbovirus infection. *PLOS Negl. Trop. Dis.* **12**, e0006247 (2018).
- S. Rosen, S. Shapouri, K. Quanbeck, B. Meade, *Food Security Assessment, 2007* (U.S. Department of Agriculture, 2008).
- Institute of Medicine, Food and Nutrition Board, *Dietary Reference Intakes: Energy, Carbohydrate, Fiber, Fat, Fatty Acids, Cholesterol, Protein, and Amino Acids* (The National Academies Press, 2005).
- V. T. Silva Gomes, E. C. Lago, N. L. C. Portela, C. N. da Cunha Santos, D. R. C. Caldas, Perfil nutricional e socioeconômico de gestantes assistidas em unidades básicas de saúde de Caxias/MA. *Rev. Interdiscip.* **8**, 127–135 (2015).
- C. A. Mourão Junior, C. Malaguti, L. de Paula Dias Moreira, N. C. Faria, W. Rezende, R. R. Rondelli, S. D. Corso, F. de Cordoba Lanza, Perfil alimentar e sócio-demográfico de gestantes adolescentes da cidade de São Paulo. *Rev. Extendere* **4**, 85–93 (2016).
- A. Hedrich, D. Novello, L. Ruviano, J. Alves, D. A. Quintiliano, Alimentary profile, nutritional and health state, and socioeconomic conditions of pregnant clients treated at the health centers in Guarapuava City, Paraná. *Rev. Salus-Guarapuava-PR.* **1**, 139–146 (2007).
- L. J. Yockey, K. A. Jurado, N. Arora, A. Millet, T. Rakib, K. M. Milano, A. K. Hastings, E. Fikrig, Y. Kong, T. L. Horvath, S. Weatherbee, H. J. Kliman, C. B. Coyne, A. Iwasaki, Type I interferons instigate fetal demise after Zika virus infection. *Sci. Immunol.* **3**, eaao1680 (2018).
- A. J. Hirsch, V. H. J. Roberts, P. L. Grigsby, N. Haese, M. C. Schabel, X. Wang, J. O. Lo, Z. Liu, C. D. Kroenke, J. L. Smith, M. Kelleher, R. Broeckel, C. N. Kreklywich, C. J. Parkins, M. Denton, P. Smith, V. DeFilippis, W. Messer, J. A. Nelson, J. D. Hennebold, M. Grafe, L. Colgin, A. Lewis, R. Ducore, T. Swanson, A. W. Legasse, M. K. Axthelm, R. MacAllister, A. V. Moses, T. K. Morgan, A. E. Frias, D. N. Streblow, Zika virus infection in pregnant rhesus macaques causes placental dysfunction and immunopathology. *Nat. Commun.* **9**, 263 (2018).
- F. M. Szaba, M. Tighe, L. W. Kummer, K. G. Lanzer, J. M. Ward, P. Lanthier, I.-J. Kim, A. Kuki, M. A. Blackman, S. J. Thomas, J.-S. Lin, Zika virus infection in immunocompetent pregnant mice causes fetal damage and placental pathology in the absence of fetal infection. *PLOS Pathog.* **14**, e1006994 (2018).

22. P. N. Gonzalez, M. Gasperowicz, J. Barbeito-Andrés, N. Klenin, J. C. Cross, B. Hallgrímsson, Chronic protein restriction in mice impacts placental function and maternal body weight before fetal growth. *PLOS ONE* **11**, e0152227 (2016).
23. S. Moussaud, H. J. Draheim, A new method to isolate microglia from adult mice and culture them for an extended period of time. *J. Neurosci. Methods* **187**, 243–253 (2010).
24. A. P. S. Rathore, W. A. A. Saron, T. Lim, N. Jahan, A. L. St. John, Maternal immunity and antibodies to dengue virus promote infection and Zika virus–induced microcephaly in fetuses. *Sci. Adv.* **5**, eaav3208 (2019).
25. J. P. Revillard, G. Cozon, Experimental models and mechanisms of immune deficiencies of nutritional origin. *Food Addit. Contam.* **7**, S82–S86 (1990).
26. R. K. Chandra, Nutrition and immunoregulation. Significance for host resistance to tumors and infectious diseases in humans and rodents. *J. Nutr.* **122**, 754–757 (1992).
27. M. Losada-Barragán, A. Umaña-Pérez, S. Cuervo-Escobar, L. R. Berbert, R. Porrozi, F. N. Morgado, D. A. Mendes-da-Cruz, W. Savino, M. Sánchez-Gómez, P. Cuervo, Protein malnutrition promotes dysregulation of molecules involved in T cell migration in the thymus of mice infected with *Leishmania infantum*. *Sci. Rep.* **7**, 45991 (2017).
28. C. Naylor, W. A. Petri Jr., Leptin regulation of immune responses. *Trends Mol. Med.* **22**, 88–98 (2016).
29. H. M. Lazear, J. Govero, A. M. Smith, D. J. Platt, E. Fernandez, J. J. Miner, M. S. Diamond, A mouse model of Zika virus pathogenesis. *Cell Host Microbe* **19**, 720–730 (2016).
30. S. L. Rossi, R. B. Tesh, S. R. Azar, A. E. Muruato, K. A. Hanley, A. J. Auguste, R. M. Langsjoen, S. Paessler, N. Vasilakis, S. C. Weaver, Characterization of a novel murine model to study Zika virus. *Am. J. Trop. Med. Hyg.* **94**, 1362–1369 (2016).
31. A. M. Paul, D. Acharya, B. Neupane, E. A. Thompson, G. Gonzalez-Fernandez, K. M. Copeland, M. Garrett, H. Liu, M. E. Lopez, M. de Cruz, A. Flynt, J. Liao, Y.-L. Guo, F. Gonzalez-Fernandez, P. J. S. Vig, F. Bai, Congenital Zika virus infection in immunocompetent mice causes postnatal growth impediment and neurobehavioral deficits. *Front. Microbiol.* **9**, 2028 (2018).
32. K.-Y. Wu, G.-L. Zuo, X.-F. Li, Q. Ye, Y.-Q. Deng, X.-Y. Huang, W.-C. Cao, C.-F. Qin, Z.-G. Luo, Vertical transmission of Zika virus targeting the radial glial cells affects cortex development of offspring mice. *Cell Res.* **26**, 645–654 (2016).
33. J. Xavier-Neto, M. Carvalho, B. d. S. Pascoalino, A. C. Cardoso, Á. M. S. Costa, A. H. M. Pereira, L. N. Santos, Á. Saito, R. E. Marques, J. H. C. Smetana, S. R. Consonni, C. Bandeira, V. V. Costa, M. C. Bajgelman, P. S. L. de Oliveira, M. T. Cordeiro, L. H. V. Gonzales Gil, B. A. Pauletti, D. C. Granato, A. F. Paes Leme, L. Freitas-Junior, C. B. M. Holanda de Freitas, M. M. Teixeira, E. Bevilacqua, K. Franchini, Hydrocephalus and arthrogryposis in an immunocompetent mouse model of ZIKA teratogeny: A developmental study. *PLOS Negl. Trop. Dis.* **11**, e0005363 (2017).
34. L. Chimelli, A. S. O. Melo, E. Avvad-Portari, C. A. Wiley, A. H. S. Camacho, V. S. Lopes, H. N. Machado, C. V. Andrade, D. C. A. Dock, M. E. Moreira, F. Tovar-Moll, P. S. Oliveira-Szejnfeld, A. C. G. Carvalho, O. N. Ugarte, A. G. M. Batista, M. M. R. Amorim, F. O. Melo, T. A. Ferreira, J. R. L. Marinho, G. S. Azevedo, J. I. B. F. Leal, R. F. M. da Costa, S. Rehen, M. B. Arruda, R. M. Brindeiro, R. Delvecchio, R. S. Aguiar, A. Tanuri, The spectrum of neuropathological changes associated with congenital Zika virus infection. *Acta Neuropathol.* **133**, 983–999 (2017).
35. A. Prata-Barbosa, M. M. Martins, A. B. Guastavino, A. J. L. A. da Cunha, Effects of Zika infection on growth. *J. Pediatr. (Rio J.)* **95**, 30–41 (2019).
36. R. Carvalho-Sauer, M. d. C. Nascimento Costa, F. R. Barreto, M. G. Teixeira, Congenital Zika syndrome: Prevalence of low birth weight and associated factors. Bahia, 2015–2017. *Int. J. Infect. Dis.* **82**, 44–50 (2019).
37. F.-M. Lum, D. K. S. Low, Y. Fan, J. J. L. Tan, B. Lee, J. K. Y. Chan, L. Rênia, F. Ginhoux, L. F. P. Ng, Zika virus infects human fetal brain microglia and induces inflammation. *Clin. Infect. Dis.* **64**, 914–920 (2017).
38. C. G. Victora, L. Adair, C. Fall, P. C. Hallal, R. Martorell, L. Richter, H. S. Sachdev; Maternal and Child Undernutrition Study Group, Maternal and child undernutrition: Consequences for adult health and human capital. *Lancet* **371**, 340–357 (2008).
39. I. Rogers, P. Emmett; ALSPAC Study Team, Diet during pregnancy in a population of pregnant women in South West England. *Eur. J. Clin. Nutr.* **52**, 246–250 (1998).
40. C. O. Schmidt, T. Kohlmann, When to use the odds ratio or the relative risk? *Int. J. Public Health* **53**, 165–167 (2008).
41. C. L. Donald, B. Brennan, S. L. Cumberworth, V. V. Rezeli, J. J. Clark, M. T. Cordeiro, R. Freitas de Oliveira França, L. J. Pena, G. S. Wilkie, A. Da Silva Filipe, C. Davis, J. Hughes, M. Varjak, M. Selinger, L. Zuvanov, A. M. Owsianka, A. H. Patel, J. McLauchlan, B. D. Lindenbach, G. Fall, A. A. Sall, R. Biek, J. Rehwinkel, E. Schnettler, A. Kohl, Full genome sequence and sRNA interferon antagonist activity of Zika virus from Recife, Brazil. *PLOS Negl. Trop. Dis.* **10**, e0005048 (2016).
42. R. S. Lanciotti, O. L. Kosoy, J. J. Laven, J. O. Velez, A. J. Lambert, A. J. Johnson, S. M. Stanfield, M. R. Duffy, Genetic and serologic properties of Zika virus associated with an epidemic, Yap State, Micronesia, 2007. *Emerg. Infect. Dis.* **14**, 1232–1239 (2008).
43. J. Schindelin, I. Arganda-Carreras, E. Frise, V. Kaynig, M. Longair, T. Pietzsch, S. Preibisch, C. Rueden, S. Saalfeld, B. Schmid, J.-Y. Tinevez, D. J. White, V. Hartenstein, K. Eliceiri, P. Tomancak, A. Cardona, Fiji: An open-source platform for biological-image analysis. *Nat. Methods* **9**, 676–682 (2012).
44. A. Dobin, T. R. Gingeras, in *Current Protocols in Bioinformatics* (John Wiley & Sons, 2015), p. 11.14.1–11.14.19.
45. H.-C. Luo, Q.-S. Luo, C.-F. Wang, M. Lei, B.-L. Li, Y.-S. Wei, Association of miR-146a, miR-149, miR-196a2, miR-499 gene polymorphisms with ischemic stroke in a Chinese people. *Oncotarget* **8**, 81295–81304 (2017).
46. B. D. Metscher, MicroCT for developmental biology: A versatile tool for high-contrast 3D imaging at histological resolutions. *Dev. Dyn.* **238**, 632–640 (2009).
47. R Foundation for Statistical Computing, R: A language and environment for statistical computing (2013); www.r-project.org/.

Acknowledgments: We thank R. Lent for support and for providing the laboratory structure to perform part of the experiments, S. I. Perez for valuable advice in different aspects of data analysis, and R. Duarte dos Santos from Departamento de Vigilância em Saúde Ambiental e Saúde do Trabalhador (DASAT/SVS) for organization and support with CID-10 and RESP data banks. H. Fuzii helped with RT-qPCR for gene validation, and E. Portiansky provided technical assistance for confocal microscopy of placenta. **Funding:** This work was funded by the MRC Zika Rapid Response Grant (MC_PC_15102), FAPERJ (E_03/2017E_03/2017), the Brazilian Ministry of Health (DASAT/SVS 25380.001612/2017-70), and the AAPA Professional Development Grant. **Author contributions:** J.B.-A. and P.P.G. conceived all experiments and wrote the manuscript. J.B.-A., J.C.C.G.F., A.A.D., and R.O.F. performed infection experiments. J.B.-A. processed the samples and analyzed the data. J.B.-A., R.V.B., and R.O.F. performed cryostat and vibratome sections and histological analyses. P.P. and A.D.R. detected ZIKV with RT-qPCR. L.M.H. propagated and titrated ZIKV. T.M.P.S. acquired µCT images. C.G.B. processed and analyzed placentas. F.F.D. performed ELISA analysis. P.C. performed hormone ELISA analyses. Z.M., L.C., R.S.A., M.T.B., M.B., A.T., F.A.L., R.T.L., C.G.B., and M.C.C. provided the laboratory structure, data, and reagents. J.M.V., C.K.N.A., M.P.C.D.S., and J.L.S.G.V. performed RNA-seq analysis. All authors discussed the results and contributed intellectually to the project. **Competing interests:** The authors declare that they have no competing interests. **Data and materials availability:** All data needed to evaluate the conclusions in the paper are present in the paper and/or the Supplementary Materials. Additional data related to this paper may be requested from the authors.

Submitted 10 January 2019

Accepted 22 October 2019

Published 10 January 2020

10.1126/sciadv.aaw6284

Citation: J. Barbeito-Andrés, P. Pezzuto, L. M. Higa, A. A. Dias, J. M. Vasconcelos, T. M. P. Santos, J. C. C. G. Ferreira, R. O. Ferreira, F. F. Dutra, A. D. Rossi, R. V. Barbosa, C. K. N. Amorim, M. P. C. De Souza, L. Chimelli, R. S. Aguiar, P. N. Gonzalez, F. A. Lara, M. C. Castro, Z. Molnár, R. T. Lopes, M. T. Bozza, J. L. S. G. Vianez, C. G. Barbeito, P. Cuervo, M. Bellio, A. Tanuri, P. P. Garcez, Congenital Zika syndrome is associated with maternal protein malnutrition. *Sci. Adv.* **6**, eaaw6284 (2020).